Spiro(fluorene-9,9′-xanthene)-Based Porous Organic Polymers: Preparation, Porosity, and Exceptional Hydrogen Uptake at Low Pressure

ARTICLE *in* MACROMOLECULES · SEPTEMBER 2011

Impact Factor: 5.8 · DOI: 10.1021/ma201626s

Macromolecules

ARTICLE

pubs.acs.org/Macromolecules

Spiro(fluorene-9,9′-xanthene)-Based Porous Organic Polymers: Preparation, Porosity, and Exceptional Hydrogen Uptake at Low Pressure

Qi Chen,[†] Jin-Xiang Wang,[†,‡] Qiu Wang,[†,§] Ning Bian,[†] Zhong-Hua Li,[§] Chao-Guo Yan,[‡] and Bao-Hang Han*[,†]

[†]National Center for Nanoscience and Technology, Beijing 100190, China

[‡]College of Chemistry & Chemical Engineering, Yangzhou University, Yangzhou 225002, China

[§]College of Chemistry, Central China Normal University, Wuhan 430079, China

Supporting Information

ABSTRACT: Preparation and sorption properties of spiro(fluorene-9,9′-xanthene)-based porous organic polymers (SPOPs) are reported for the first time. Using a same linker monomer, the micropore size and specific surface area in SPOPs are tunable by variation of the structure of core building blocks. According to the obtained nitrogen physisorption isotherms, the Brunauer–Emmett–Teller specific surface area for these polymers varies between 750 and 1020 $m^2 g^{-1}$. Copolymer SPOP-3 containing spiro(fluorene-9,9′-xanthene) and spirobifluorene with 1:1 ratio, prepared through Suzuki coupling polymerization, possesses 2.22 wt % hydrogen adsorption capacity at 1.0 bar and 77 K, which not only is the exceptional uptake capacity for hydrogen at low pressure among the best reported results for organic polymers but also can be competitive with other kinds of porous materials such as activated carbons and metal–organic frameworks.

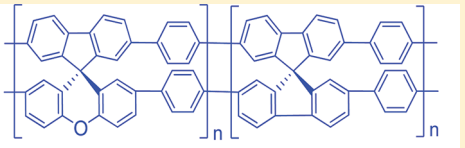

Porous organic polymer (S_{BET} = ~1000 $m^2 g^{-1}$) with the exceptional H_2 uptake capacity (2.22 wt %) at 1 bar and 77 K

INTRODUCTION

As a promising porous material with potential application in heterogeneous catalysis[1] and gas storage,[2] versatile porous organic polymers (POPs) were obtained efficiently by selection of proper building blocks, which show high flexibility in the molecular design.[3] Due to the rigid and contorted structure, aromatic spirocyclic compounds have been used as wonderful building blocks in preparation of POPs such as solution-processable polymers of intrinsic microporosity (PIMs)[4] and conjugated microporous polymers (CMPs) with large specific surface area.[5] Especially, spirobifluorene derivatives with a perpendicular arrangement structure of two biphenylene planes possess a superior morphological stability, which is a novel core building unit to produce a contorted polymeric structure.[6] It is reported that the Brunauer–Emmett–Teller (BET) specific surface area of spirobifluorene-based porous polymer is above 1000 $m^2 g^{-1}$.[7]

Spiro(fluorene-9,9′-xanthene) (SFX), as a spiro-structured compound containing heteroatoms in the spiro-skeleton, is a typical building unit used in organic optoelectronic materials owing to its high thermal and oxidative stability.[8] As for the molecular structure of SFX, the fluorene and xanthene moieties are positioned in a nearly planar conformation and connected through the tetrasubstituted carbon atom spiro-center. Meanwhile, the planes of the two moieties are arranged orthogonally (dihedral angle = 89.8°),[8a] which is similar to the configuration of spirobifluorene. Furthermore, introducing a heteroatom into porous polymers can modify the electron conductivity of the conjugated polymer backbone, which may enhance the dipole–dipole interaction between sorbate molecule and adsorbent.[7] Considering its easy preparation and intrinsic structure, we believe that SFX is expected to be a novel building block for design of conjugated porous polymers with special properties. In this paper, preparation and sorption properties of SFX-based porous organic polymers are reported. Polymer synthesis is facilitated smoothly by palladium-catalyzed C–C coupling polycondensation. The BET specific surface area for these polymers ranges from 750 to 1020 $m^2 g^{-1}$. Gravimetric hydrogen adsorption isotherms show that the hydrogen uptake of the synthetic SPOPs is up to 2.22 wt % at 1.0 bar and 77 K, which is a high uptake capacity for hydrogen at low pressure among the best reported results for organic polymers under the same conditions.

EXPERIMENTAL SECTION

Materials and Measurements. All chemical reagents were commercially available and used as received unless otherwise stated. Benzene-1,4-diboronic acid (BDBA), 1,4-diethynylbenzene, and tetrakis(triphenylphosphine)palladium(0) were purchased from Acros. Spiro(fluorene-9,9′-xanthene)[9] and 2,2′,7,7′-tetrabromo-9,9′-spirobifluorene (TBSBF)[10] were prepared according to reported methods, respectively.

Received: July 15, 2011
Revised: September 3, 2011
Published: September 28, 2011

Scheme 1. Preparation of SPOPs by Palladium-Catalyzed C−C Coupling Polycondensation

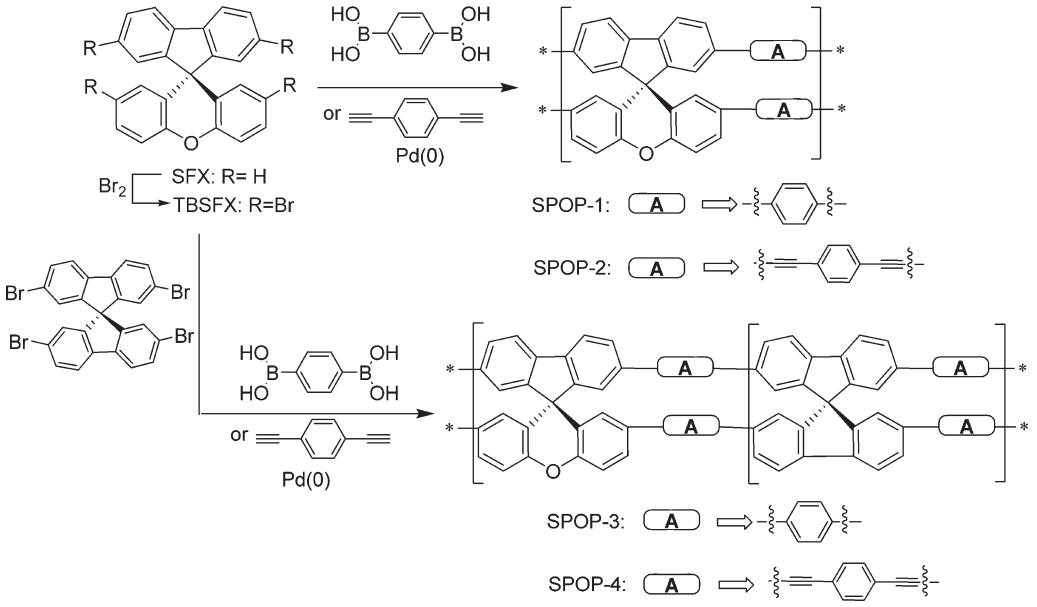

The ^{1}H and ^{13}C NMR spectra were recorded on a Bruker DMX400 NMR spectrometer. Solid-state cross-polarization magic angle spinning (CP/MAS) NMR spectra were recorded on a Bruker Avance III 400 NMR spectrometer. Nitrogen sorption isotherms were obtained with a Micromeritics ASAP 2020 M+C accelerated surface area and porosimetry analyzer at 77 K. The samples were degassed overnight at 120 °C. The obtained adsorption−desorption isotherms were evaluated to give the pore parameters, including BET specific surface area, pore size, and pore volume. The pore size distribution was calculated from the adsorption branch with the nonlocal density function theory (NLDFT) approach. SEM observations were carried out using a Hitachi S-4800 microscope (Hitachi Ltd., Japan) at an accelerating voltage of 6.0 kV and equipped with a Horiba energy dispersive X-ray spectrometer. TEM observations were carried out using a Tecnai G^2 20 S-TWIN microscope (FEI) at an accelerating voltage of 200 kV. The infrared (IR) spectra were recorded using a PerkinElmer Spectrum One FT-IR spectrometer. X-ray diffraction (XRD) patterns of the samples were acquired from 0.5° to 35° by a Philips X′Pert PRO X-ray diffraction instrument. The fluorescence spectra were measured using a PerkinElmer LS55 luminescence spectrometer.

Synthesis of Tetrabromospiro(fluorene-9,9′-xanthene) (TBSFX). To a solution of spiro(fluorene-9,9′-xanthene) (333 mg, 1.0 mmol) in chloroform (8.0 mL) at 0 °C were added ferric chloride (8 mg, 0.05 mmol) and bromine (0.4 mL, 4.1 mmol). The solution was warmed to room temperature and stirred for 3 h. After poured into water (50 mL), the resulting mixture was washed with saturated sodium thiosulfate until the red color disappeared. The aqueous layer was extracted with dichloromethane (2 × 50 mL), and then the combined organic layer was dried over sodium sulfate and concentrated under reduced pressure to give TBSFX as a white solid (615 mg, 95%), which is pure enough for further use. Mp 246−248 °C. ^{1}H NMR (400 MHz, $CDCl_3$): δ 7.66 (d, J = 8.4 Hz, 2H), 7.56 (dd, J_1 = 8.0 Hz, J_2 = 1.6 Hz, 2H), 7.35 (dd, J_1 = 8.4 Hz, J_2 = 2.0 Hz, 2H), 7.23 (d, J = 1.6 Hz, 2H), 7.13 (d, J = 8.8 Hz, 2H), 6.44 (d, J = 2.4 Hz, 2H). ^{13}C NMR (100 MHz, $CDCl_3$): δ 155.5, 150.0, 137.5, 133.0, 132.2, 130.3, 129.0, 124.8, 122.9, 121.9, 119.1, 116.2, 58.6.

Synthesis of SPOP-1 and SPOP-3 by Suzuki Coupling Polymerization. SPOP-1 and SPOP-3 were synthesized by palladium-catalyzed Suzuki coupling condensation reaction between BDBA and arylbromide. A representative preparation for SPOP-3 is given in details as follows:

A mixture of TBSFX (162 mg, 0.25 mmol), 2,2′,7,7′-tetrabromo-9,9′-spirobifluorene (158 mg, 0.25 mmol), and BDBA (163 mg, 1.0 mmol) in dimethylformamide (DMF, 100 mL) was degassed by the freeze−pump−thaw cycles. To the mixture were added an aqueous solution of potassium carbonate (2.0 M, 16 mL) and tetrakis(triphenylphosphine)palladium(0) (50 mg, 55 μmol). The resulting solution was degassed and purged with nitrogen and stirred at 150 °C for 36 h. The mixture was cooled to room temperature and poured into water. The insoluble precipitate was filtered and washed with water, methanol, and acetone to remove any unreacted monomers or catalyst residues. Further purification of the polymer was carried out by Soxhlet extraction with water, methanol, and tetrahydrofuran (THF) for 24 h to give SPOP-3 (230 mg) as a solid.

As for SPOP-1, only TBSFX was used as core structure monomer, and its amount is a half-equivalence of BDBA. SPOP-1 can be obtained according to the procedure as described above.

Synthesis of SPOP-2 and SPOP-4 by Sonogashira−Hagihara Coupling Polymerization. SPOP-2 and SPOP-4 were synthesized by palladium-catalyzed Sonogashira−Hagihara coupling condensation reaction between 1,4-diethynylbenzene and aryl bromide. A representative preparation for SPOP-4 is given in details as follows:

1,4-Diethynylbenzene (126 mg, 1 mmol), TBSFX (162 mg, 0.25 mmol), and 2,2′,7,7′-tetrabromo-9,9′-spirobifluorene (158 mg, 0.25 mmol) were dissolved in the mixture of DMF (25 mL) and triethylamine (25 mL), and then the mixture was degassed by the freeze−pump−thaw cycles. To the mixture were added tetrakis(triphenylphosphine)palladium(0) (30 mg) and copper(I) iodide (10 mg). The resulting mixture was heated to 90 °C and stirred for 72 h under a nitrogen atmosphere. After cooled to room temperature, the insoluble precipitate was filtered and washed three times with water, dichloromethane, and methanol to remove any unreacted monomers or catalyst residues. Further purification of the polymer was carried out by Soxhlet extraction with water, methanol, and tetrahydrofuran for 72 h. The product was then dried under vacuum for 24 h at 120 °C to give a brown powder (280 mg).

As for SPOP-2, only TBSFX was used as core structure monomer, and its amount is a half-equivalence of 1,4-diethynylbenzene.

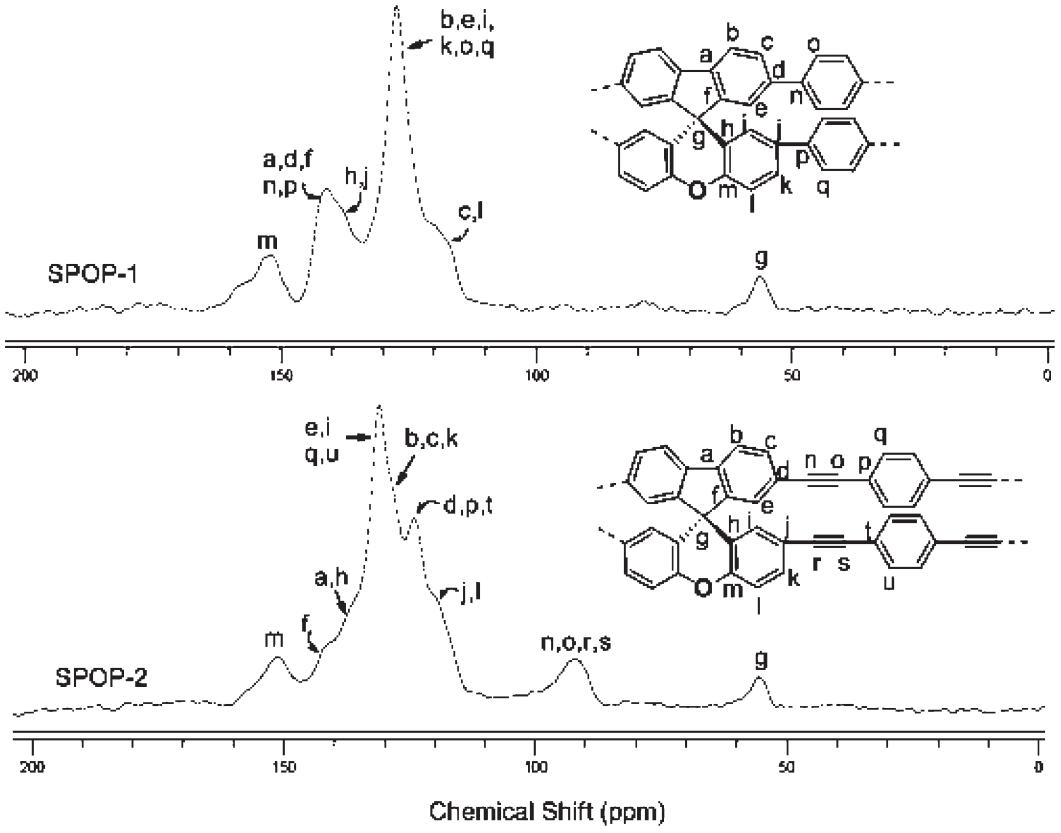

Figure 1. ^{13}C CP/MAS NMR spectra of SPOP-1 and SPOP-2.

SPOP-2 can be obtained according to the procedure as described above.

RESULTS AND DISCUSSION

SFX can be efficiently prepared on a large scale according to Huang's method. After bromination with bromine, tetrabromo-substituted SFX (TBSFX) is obtained in a high yield, which is a core monomer for construction of porous organic polymers with potential applications. As shown in Scheme 1, SPOP-1 and SPOP-2 can be prepared in high yields from TBSFX through Suzuki coupling polymerization and Sonogashira−Hagihara coupling polymerization, which are reliable methods to furnish POPs proved by Thomas[6] and Cooper,[11] respectively. Since the monomer structures show a significant influence on the surface property and porous structure of porous polymers,[12] 2,2′,7,7′-tetrabromo-9,9′-spirobifluorene (TBSBF) as another contorted or nonplanar core monomer with similar reactivity has been selected to prepare two porous copolymers (SPOP-3 and SPOP-4) containing SFX and 9,9′-spirobifluorene (SBF) with 1:1 ratio using the same methods.

All polymers were characterized at the molecular level by the ^{13}C CP/MAS NMR spectrum. The ^{13}C NMR spectra for the porous polymers with assignment of the resonances are shown in Figure 1. For SPOP-1, there are four broad peaks at approximately 152.0, 141.0, 127.3, and 56.3 ppm, respectively. The low-intensity peak at 152.0 ppm corresponds to the substituted phenyl carbons binding with oxygen atom. The broad peak at 141.0 ppm with a shoulder at 139.0 ppm corresponds to the other substituted phenyl carbons, in which the signal peak of the other substituted phenyl carbons in the xanthene moiety is ascribed to the shoulder peak at 139.0 ppm. The signal peak for unsubstituted phenyl carbons is located at 127.3 ppm, which is including a broad shoulder peak at 118.5 ppm. In addition, the observed signal intensity at 56.3 ppm is ascribed to the quaternary carbons in SFX moieties. As to SPOP-2, the peak at 151.2 ppm corresponds to the substituted phenyl carbons binding with oxygen atom and the shoulder peaks at 140.5 and 138.5 ppm correspond to the other substituted phenyl carbons (in the SFX moiety) linking to non-acetylene groups. The high signal intensity at about 131.0 ppm shows the most of unsubstituted phenyl carbons. As shown in Figure 1, two shoulder peaks at 123.4 and 119.0 ppm correspond to all the acetylene-substituted phenyl carbons and the rest of unsubstituted phenyl carbons in the SFX moiety. Furthermore, the broad low-intensity peak at ∼92.2 ppm is ascribed to acetylene carbons. The signal peak of quaternary carbons in SFX moieties is still observed at 55.6 ppm similarly. The ^{13}C CP/MAS NMR spectra for the triple-bond linkage of the SPOP-2 and SPOP-4 are also consistent with the data obtained by FT-IR measurement, in which the triple bond of acetylene carbon yields the signal at about 2350 cm^{-1} (Supporting Information, Figure S1). As for copolymers SPOP-3 and SPOP-4, their ^{13}C CP/MAS NMR spectra are shown in Figure S2 (Supporting Information) with a similar signal distribution.

The porosity parameters of the polymers were studied by sorption analysis using nitrogen as the sorbate molecule. Nitrogen adsorption−desorption isotherms of SPOPs measured at 77 K are shown in Figure 2. SPOP-1 possesses a type I nitrogen gas sorption isotherm according to the IUPAC classification[13] and shows a very flat sorption plateau, indicating that the material is microporous. SPOP-2 and SPOP-4 exhibit similar nitrogen gas

sorption isotherms compared with SPOP-1. The nitrogen isotherm for SPOP-3 differs substantially at the high relative pressure range and exhibits a combination of type I and II nitrogen sorption isotherms. The increase in the nitrogen sorption at a high relative pressure above 0.9 may arise in part from interparticulate porosity associated with the meso- and macrostructures of the samples and interparticular void.[14] In addition, hysteresis can be observed for the whole range of relative pressure based on the isotherms due to a linear increase of the adsorbed volume upon adsorption, which might be attributed to the swelling in a flexible polymer framework induced by adsorbate molecules dissolved in nominally nonporous parts of the polymer matrix after filling of open and accessible voids[15] or the restricted access of adsorbate to the pores blocked by narrow openings.[16]

Listed in Table 1 are the key structural properties derived from the isotherm, such as the Brunauer–Emmett–Teller (BET) and Langmuir specific surface area, micropore surface area, and pore volumes. As for determination of the specific surface area, the relative pressure range (P/P_0) commonly used is 0.05–0.2. However, in some cases, it can not give a good fit for microporous materials.[17] Alternatively, a narrower pressure range at $P/P_0 < 0.1$ instead of 0.05–0.2 is used.[17b] The BET specific surface area values for SPOPs calculated over these two different pressure ranges (Supporting Information, Figures S3–S6) are found to be close to each other. The BET specific surface area for these polymers ranges from 750 to 1020 $m^2\ g^{-1}$, which is calculated in the relative pressure (P/P_0) range from 0.01 to 0.1 according to the previous reports[15,17] (Supporting Information, Table S1). It should be noted that when TBSFX was used as the only core monomer, the obtained homopolymers (SPOP-1 and SPOP-2) show a moderate BET specific surface area (~750 $m^2\ g^{-1}$). A similar result was found by Weber and Thomas for homopolymers P1 (450 $m^2\ g^{-1}$) and P3 (510 $m^2\ g^{-1}$) obtained using the same method,[6] in which only TBSBF is the core monomer. However, when the same amounts of TBSFX and TBSBF are used as core constructing monomers together, the BET specific surface area of both synthetic copolymers (SPOP-3 and SPOP-4) improve to about 1000 $m^2\ g^{-1}$. Meanwhile, the micropore surface area, total pore volume, and micropore volume of copolymers show correspondingly improving trends. For the nonordered porous materials, accurate determination of the pore size distribution (PSD) is very difficult. Different results are usually obtained according to different calculation methods. PSD analysis based on the NLDFT approach has been used extensively to characterize a wide variety of porous materials although it does have limitations.[15] However, the calculated results can give us some related qualitative information, with which one can make a relative comparison of materials synthesized from different monomers. The pore size distribution of all polymers was calculated from the adsorption branch of the isotherms with the NLDFT approach. As shown in Figure 3 and Table 1, the dominant pore size of homopolymer SPOP-1 is centered at 0.54 and 1.27 nm, respectively. When half amount of SFX is replaced by SBF as the core constructing monomer, the dominant pore size of the obtained copolymer SPOP-3 shifts to 0.68 and 1.26 nm, respectively. The pore size distribution for SPOP-2 and SPOP-4 are shown in Figure S7 (Supporting Information), in which two polymers exhibit a similar pore size distribution

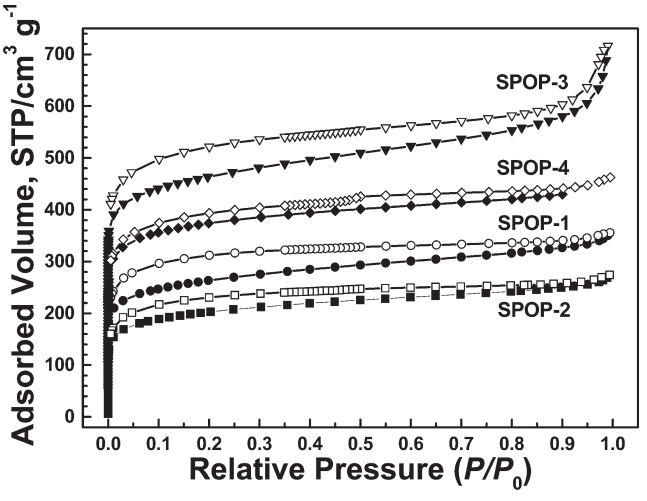

Figure 2. Nitrogen adsorption–desorption isotherms of SPOPs measured at 77 K (the adsorption and desorption branches are labeled with solid and open symbols, respectively). For clarity, the isotherms of SPOP-3, SPOP-4, and SPOP-1 were shifted vertically by 200, 100, and 50 $cm^3\ g^{-1}$, respectively.

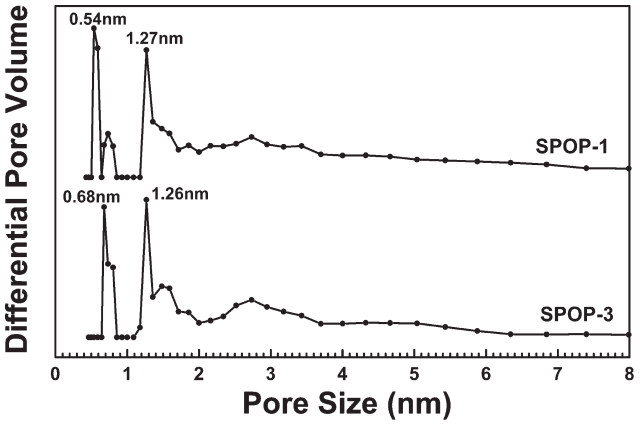

Figure 3. Pore size distribution of SPOP-1 and SPOP-3 calculated by NLDFT.

Table 1. Porosity Properties and Gas Uptake Capacities of Polymers

SPOPs	S_{BET} ($m^2\ g^{-1}$)[a]	S_{micro} ($m^2\ g^{-1}$)[b]	V_{total} ($cm^3\ g^{-1}$)[c]	dominant pore diameter (nm)[d]	CO_2 uptake (wt %)[e]	hydrogen uptake (wt %)[f]
SPOP-1	784 (884)	425	0.449	0.54, 1.27	11.3	1.20
SPOP-2	750 (846)	396	0.403	0.59	9.44	1.05
SPOP-3	965 (1089)	431	0.690	0.68, 1.26	11.6	2.22
SPOP-4	1020 (1148)	636	0.533	0.59	12.0	1.67

[a] Specific surface area calculated from the nitrogen adsorption isotherm using the BET method. The number in parentheses is the Langmuir specific surface area calculated from the nitrogen adsorption isotherm by application of the Langmuir equation. [b] Micropore surface area calculated from the nitrogen adsorption isotherm using the *t*-plot method. [c] Total pore volume at $P/P_0 = 0.97$. [d] Data calculated from nitrogen adsorption isotherms with the nonlocal density function theory (NLDFT) method. [e] Data were obtained at 1.0 bar and 273 K. [f] Data were obtained at 1.0 bar and 77 K.

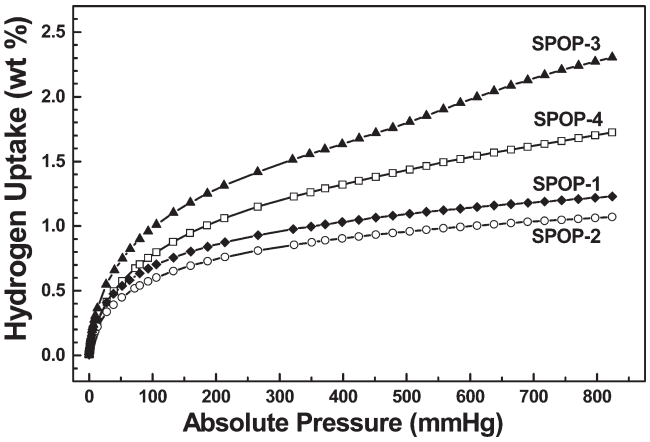

Figure 4. Gravimetric hydrogen adsorption isotherms for SPOPs at 77 K.

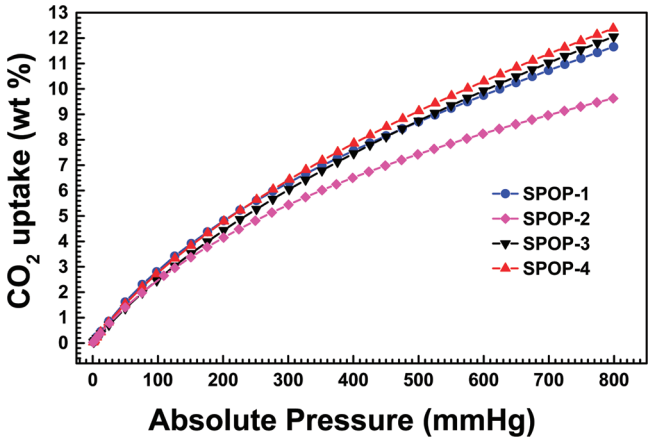

Figure 5. Gravimetric CO_2 adsorption isotherms for SPOPs at 273 K.

around 0.59 nm. Those results indicate that using a same linker monomer, to some extent, the micropore size and specific surface area of POPs are tunable by variation of the core building blocks.

Conjugated POPs with a narrow pore distribution may interact attractively with small gas molecules through improved molecular interaction. On account of the high capacity in hydrogen adsorption for many porous materials, we investigated the hydrogen uptake of SPOPs based on the hydrogen physisorption isotherms measured at 77 K and a pressure up to 1.13 bar (Figure 4). An increase in the hydrogen loading capacity with increasing specific surface area is observed with exception for SPOP-3. SPOP-2, possessing the lowest BET specific surface area and the lowest total pore volume among the prepared SPOPs, exhibits the lowest hydrogen uptake of 1.05 wt % at 1.0 bar and 77 K. As for SPOP-4 with high specific surface area (S_{BET} = 1020 m^2 g^{-1}), its hydrogen uptake is up to 1.67 wt % under the same condition. These data indicate that the specific surface area of porous polymer shows a significant effect on the hydrogen uptake. The hydrogen uptake capacity of SPOP-4 not only can be comparable to triptycene-based porous polymer Trip(Me)-PIMs[18] (1.79 wt % at 1 bar, 77 K, S_{BET} = 1760 m^2 g^{-1}) reported recently, the conjugated microporous polymer based on spiro-bipropylenedioxythiophene SPT-CMP 2[5a] (1.57 wt % at 1.13 bar, 77 K, S_{BET} = 1601 m^2 g^{-1}), and porous polyporphyrin containing Fe−porphyrin complex P(Fe−TTPP)[19] (~1.5 wt % at 1 bar, 77 K, S_{BET} = 1248 m^2 g^{-1}), but also is higher than the porous polymers with higher BET specific surface area, for example, the element organic framework EOF-6[14] (1.29 wt % at 1 bar, 77 K, S_{BET} = 1380 m^2 g^{-1}) obtained previously, imine-linked microporous polymer organic framework POF A1-B2[20] (1.5 wt % at 1 bar, 77 K, S_{BET} = 1380 m^2 g^{-1}), and adamantane-based porous polymer network PPN-3[21] (1.58 wt % at 1 bar, 77 K, S_{BET} = 2840 m^2 g^{-1}). These results prove that, besides the specific surface area, the molecular structure and chemical nature of the monomer also play crucial roles in the hydrogen uptake capacity of the POPs. Therefore, selection of proper building blocks is an important basis for synthetic porous polymer designing. The uptake capacity of SPOPs for carbon dioxide is also studied. From the carbon dioxide physisorption isotherms measured at 273 K and a pressure up to 1.13 bar (Figure 5), we can find an increasing trend in the carbon dioxide loading capacity with increasing specific surface area (Table 1). SPOP-4, possessing the highest BET specific surface area, exhibits the highest carbon dioxide storage of 12.0 wt % at 1.0 bar and 273 K.

Table 2. Summary of the High Uptake Capacities of Various Porous Materials for Hydrogen at Low Pressure and 77 K

porous materials	S_{BET} (m^2 g^{-1})	hydrogen uptake (wt %, 1 bar)	ref
SPOP-3	967	2.22	
SPOP-4	1035	1.67	
Trip(Me)-PIM	1760	1.80	18
Trip(*i*-Pr)-PIM	1601	1.83	18
SPT-CMP 2	1601	~1.52	5a
PPN-3	2840	1.58	21
PAF-1	5600	~1.50	24a
COF-5	1590	0.9	24b
COF-102	3620	1.20	24b
carbon AX-21	2421	2.40	22a
zeolite-like carbon	3200	2.60	22b
MOF-505	1670	2.59	23a
MIL-101	5500	2.50	23b

McKeown and co-workers have reported recently that the loading value of hydrogen at low pressure (1 bar) within Trip(i-Pr)-PIM[18] (S_{BET} = 1601 m^2 g^{-1}) is 1.83 wt % at 77 K, which is the highest reported value for POPs. It is impressive that the hydrogen uptake capacity of SPOP-3 is 2.22 wt % under the same condition, which is higher than Trip(i-Pr)-PIM. Furthermore, the loading value of hydrogen for SPOP-3 at low pressure can be competitive with other kinds of porous materials such as activated carbons[22] and metal−organic frameworks (MOFs).[23] Comparison of the high hydrogen uptake capacities of various porous materials[18,24] with SPOP-3 and SPOP-4 at low pressure and 77 K is listed in Table 2. Though the specific surface area of SPOP-3 (S_{BET} = 965 m^2 g^{-1}) is slightly lower than SPOP-4, its hydrogen uptake capacity is apparently much higher than SPOP-4. This confirms that specific surface area is not the only criterion for hydrogen adsorption. It has been reported previously that pores of diameter in the range of 0.6−0.8 nm are optimal for hydrogen physisorption at low pressures for various microporous materials.[18,25] The dominant pore size distribution of prepared SPOP-3, as aforementioned, is located at 0.68 and 1.26 nm, which is suitable for multilayer adsorption. From the hydrogen physisorption isotherms, we can see that SPOP-3 seems to follow a linear increasing uptake at higher pressures, while the others are inclined to level off. This suggests that, as the

dx.doi.org/10.1021/ma201626s |*Macromolecules* 2011, 44, 7987–7993

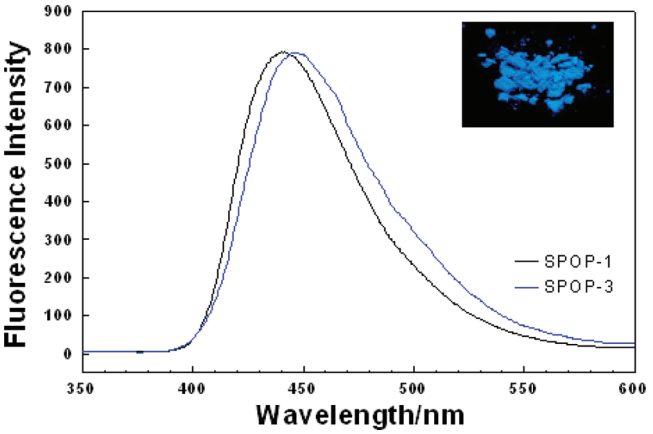

Figure 6. Fluorescent spectra of SPOP-1 and SPOP-3 in solid-state and photo of SPOP-1 under UV light (365 nm) illumination.

randomly packed network, conformation change of the polymer has probably taken place with enhancing pressure, due to rotation and stretching of the building units, which may provide some "hidden" micropores and surface area in the polymer for hydrogen to continually permeate into this material. Thanks to the high specific surface area, special core structure containing heteroatoms in the spiro-skeleton, and dominant pore size distribution at 0.6−0.8 nm, SPOP-3 possesses the exceptional uptake capacity for hydrogen at low pressure among the best reported results for porous organic polymers.

SFX-based porous polymers obtained through Suzuki coupling polymerization exhibit strong photoluminescence properties. SPOP-1 and SPOP-3 show blue emission with a maximum wavelength at about 450 nm (Figure 6). As expected, all SFX-based nanoporous organic polymers show a nonordered, amorphous structure proved by the X-ray diffraction (XRD) measurements due to the kinetic control of the polymerization. Figures S8 and S9 (Supporting Information) show scanning electron microscopy images and high-resolution transmission electron microscopy images of polymer SPOP-1. SEM analysis of SPOP-1 displays that the polymer consist of uniform solid submicrometer spheres with particle sizes about 410 nm. Small macropores or mesopores in the polymers can be ascribed mostly to the interparticulate porosity existing between agglomerated microgel particles.[26] The TEM images are indicative of porous structures of the materials, which are similar to some reported amorphous microporous organic polymers.

CONCLUSION

SFX-based porous organic polymers were prepared smoothly by palladium-catalyzed C−C coupling polycondensation using either TBSFX or TBSFX and TBSBF with 1:1 ratio as core building units. The specific surface area and micropore size of the prepared SPOPs are tunable by variation of the core building block. The BET specific surface area for these polymers is high up to 1020 m^2 g^{-1}. Gravimetric hydrogen adsorption isotherms show that the adsorption capacity of SPOP-3 for hydrogen is 2.22 wt % at 1.0 bar and 77 K, which not only is a high uptake capacity for hydrogen at low pressure among the best reported results for POPs but also can be competitive with other kinds of porous materials such as activated carbons and MOFs. The high hydrogen uptake capacity of SPOP-3 at low pressure can be ascribed to its high specific surface area, special core structure containing heteroatoms in the spiro-skeleton, and dominant pore size distribution at 0.6−0.8 nm, which may provide some clues for the designing of porous material used for gas storage.

ASSOCIATED CONTENT

Supporting Information. FT-IR spectra of SPOP-2 and SPOP-4; ^{13}C CP/MAS NMR spectra of SPOP-3 and SPOP-4; BET specific surface areas of SPOPs calculated over different pressure ranges; pore size distribution of SPOP-2 and SPOP-4 calculated by NLDFT; SEM and TEM images of SPOP-1; ^{1}H NMR and ^{13}C NMR of TBSFX. This material is available free of charge via the Internet at http://pubs.acs.org.

AUTHOR INFORMATION

Corresponding Author
*Tel: +86 10 8254 5576. E-mail: hanbh@nanoctr.cn.

ACKNOWLEDGMENT

The financial support of the Ministry of Science and Technology of China (Grant 2011CB932500), National Science Foundation of China (Grants 20972035, 91023001, and 21002017), and the Chinese Academy of Sciences (Grant KJCX2-YW-H21) is acknowledged.

REFERENCES

(1) (a) Chen, L.; Yang, Y.; Jiang, D. *J. Am. Chem. Soc.* **2010**, *132* (26), 9138–9143. (b) Du, X.; Sun, Y.; Tan, B.; Teng, Q.; Yao, X.; Su, C.; Wang, W. *Chem. Commun.* **2010**, *46* (6), 970–972.

(2) (a) Doonan, C. J.; Tranchemontagne, D. J.; Glover, T. G.; Hunt, J. R.; Yaghi, O. M. *Nature Chem.* **2010**, *2* (3), 235–238. (b) Choi, J. H.; Choi, K. M.; Jeon, H. J.; Choi, Y. J.; Lee, Y.; Kang, J. K. *Macromolecules* **2010**, *43* (13), 5508–5511. (c) Germain, J.; Frechét, J. M. J.; Svec, F. *Small* **2009**, *5* (10), 1098–1111.

(3) (a) Cooper, A. I. *Adv. Mater.* **2009**, *21* (12), 1291–1295. (b) McKeown, N. B.; Budd, P. M. *Macromolecules* **2010**, *43* (12), 5163–5176. (c) Chen, Q.; Luo, M.; Wang, T.; Wang, J.-X.; Zhou, D.; Han, Y.; Yan, C.-G.; Han., B.-H. *Macromolecules* **2011**, *44* (14), 5573–5577. (d) Zhao, Y.-C.; Zhou, D.; Chen, Q.; Zhang, X.-J.; Bian, N.; Qi, A.-D.; Han, B.-H. *Macromolecules* **2011**, *44* (16), 6382–6388.

(4) Budd, P. M.; Elabas, E. S.; Ghanem, B. S.; Makhseed, S.; McKeown, N. B.; Msayib, K.; Tattershall, C. E.; Wang, D. *Adv. Mater.* **2004**, *16* (5), 456–459.

(5) (a) Jiang, J. X.; Laybourn, A.; Clowes, R.; Khimyak, Y. Z.; Bacsa, J.; Higgins, S. J.; Adams, D. J.; Cooper, A. I. *Macromolecules* **2010**, *43* (18), 7577–7582. (b) Weber, J.; Antonietti, M.; Thomas, A. *Macromolecules* **2008**, *41* (8), 2880–2885.

(6) Weber, J.; Thomas, A. *J. Am. Chem. Soc.* **2008**, *130* (20), 6334–6335.

(7) Yuan, S.; Kirklin, S.; Dorney, B.; Liu, D.-J.; Yu, L. *Macromolecules* **2009**, *42* (5), 1554–1559.

(8) (a) Tseng, Y. H.; Shih, P. I.; Chien, C. H.; Dixit, A. K.; Shu, C. F.; Liu, Y. H.; Lee, G. H. *Macromolecules* **2005**, *38* (24), 10055–10060. (b) McFarlane, S. L.; Coumont, L. S.; Piercey, D. G.; McDonald, R.; Veinot, J. G. C. *Macromolecules* **2008**, *41* (21), 7780–7782. (c) Chu, Z.; Wang, D.; Zhang, C.; Fan, X.; Tang, Y.; Chen, L.; Zou, D. *Macromol. Rapid Commun.* **2009**, *30* (20), 1745–1750.

(9) Xie, L.-H.; Liu, F.; Tang, C.; Hou, X.-Y.; Hua, Y.-R.; Fan, Q.-L.; Huang, W. *Org. Lett.* **2006**, *8* (13), 2787–2790.

(10) Wu, R. L.; Schumm, J. S.; Pearson, D. L.; Tour, J. M. *J. Org. Chem.* **1996**, *61* (20), 6906–6921.

(11) Jiang, J. X.; Su, F.; Trewin, A.; Wood, C. D.; Campbell, N. L.; Niu, H.; Dickinson, C.; Ganin, A. Y.; Rosseinsky, M. J.; Khimyak, Y. Z.; Cooper, A. I. *Angew. Chem., Int. Ed.* **2007**, *46* (45), 8574–8578.
(12) Jiang, J. X.; Su, F.; Trewin, A.; Wood, C. D.; Niu, H.; Jones, J. T. A.; Khimyak, Y. Z.; Cooper, A. I. *J. Am. Chem. Soc.* **2008**, *130* (24), 7710–7720.
(13) Sing, K. S. W.; Everett, D. H.; Haul, R. A. W.; Moscou, L.; Pierotti, R. A.; Rouquérol, J.; Siemieniewska, T. *Pure Appl. Chem.* **1985**, *57* (4), 603–619.
(14) Rose, M.; Klein, N.; Böhlmann, W.; Böhringer, B.; Fichtner, S.; Kaskel, S. *Soft Mater.* **2010**, *6* (16), 3918–3923.
(15) Weber, J.; Schmidt, J.; Thomas, A.; Böhlmann, W. *Langmuir* **2010**, *26* (19), 15650–15656.
(16) Rose, M.; Böhlmann, W.; Sabo, M.; Kaskel, S. *Chem. Commun.* **2008**, *44* (21), 2462–2464.
(17) (a) Walton, K. S.; Snurr, R. Q. *J. Am. Chem. Soc.* **2007**, *129* (27), 8552–8556. (b) Dawson, R.; Laybourn, A.; Clowes, R.; Khimyak, Y. Z.; Adams, D. J.; Cooper, A. I. *Macromolecules* **2009**, *42* (22), 8809–8816.
(18) Ghanem, B. S.; Hashem, M.; Harris, K. D. M.; Msayib, K. J.; Xu, M.; Budd, P. M.; Chaukura, N.; Book, D.; Tedds, S.; Walton, A.; McKeown, N. B. *Macromolecules* **2010**, *43* (12), 5287–5294.
(19) Xia, J.; Yuan, S.; Wang, Z.; Kirklin, S.; Dorney, B.; Liu, D.-J.; Yu, L. *Macromolecules* **2010**, *43* (7), 3325–3330.
(20) Pandey, P.; Katsoulidis, A. P.; Eryazici, I.; Wu, Y.; Kanatzidis, M. G.; Nguyen, S. T. *Chem. Mater.* **2010**, *22* (17), 4974–4979.
(21) Lu, W.; Yuan, D.; Zhao, D.; Schilling, C. I.; Plietzsch, O.; Muller, T.; Bräse, S.; Guenther, J.; Blümel, J.; Krishna, R.; Li, Z.; Zhou, H.-C. *Chem. Mater.* **2010**, *22* (21), 5964–5972.
(22) (a) Texier-Mandoki, N.; Dentzer, J.; Piquero, T.; Saadallah, S.; David, P.; Vix-Guterl, C. *Carbon* **2004**, *42* (13), 2744–2747. (b) Yang, Z. X.; Xia, Y. D.; Mokaya, R. *J. Am. Chem. Soc.* **2007**, *129* (6), 1673–1679.
(23) (a) Lin, X.; Jia, J. H.; Zhao, X. B.; Thomas, K. M.; Blake, A. J.; Walker, G. S.; Champness, N. R.; Hubberstey, P.; Schroder, M. *Angew. Chem., Int. Ed.* **2006**, *45* (44), 7358–7364. (b) Latroche, M.; Surble, S.; Serre, C.; Mellot-Draznieks, C.; Llewellyn, P. L.; Lee, J .H.; Chang, J. S.; Jhung, S. H.; Ferey, G. *Angew. Chem., Int. Ed.* **2006**, *45* (48), 8227–8231.
(24) (a) Ben, T.; Rao, H.; Ma, S.; Cao, D.; Lan, J.; Jing, X.; Wang, W.; Xu, J.; Deng, F.; Simmons, J. M.; Qui, S.; Zhu, G. *Angew. Chem., Int. Ed.* **2009**, *48* (50), 9457–9460. (b) Furukawa, H.; Yaghi, O. M. *J. Am. Chem. Soc.* **2009**, *131* (25), 8875–8883.
(25) Germain, J.; Svec, F.; Frechét, J. M. J. *Chem. Mater.* **2008**, *20* (22), 7069–7076.
(26) Jiang, J.-X.; Su, F.; Niu, H.; Wood, C. D.; Campbell, N. L.; Khimyak, Y. Z.; Cooper, A. I. *Chem. Commun.* **2008**, *44* (4), 486–488.